



# CHORUS

This is the accepted manuscript made available via CHORUS. The article has been published as:

## Electronic structure of the topological superconductor candidate $\text{Au}_{2}\text{Pb}$

Yun Wu, Gil Drachuck, Lin-Lin Wang, Duane D. Johnson, Przemyslaw Swatek, Benjamin Schruck, Daixiang Mou, Lunan Huang, S. L. Bud'ko, P. C. Canfield, and Adam Kaminski

Phys. Rev. B **98**, 161107 — Published 9 October 2018

DOI: [10.1103/PhysRevB.98.161107](https://doi.org/10.1103/PhysRevB.98.161107)

# Electronic structure of topological superconductor candidate $\text{Au}_2\text{Pb}$

Yun Wu,<sup>1,2</sup> Gil Drachuck,<sup>1,2</sup> Lin-Lin Wang,<sup>1</sup> Duane. D. Johnson,<sup>1,2,3</sup> Przemyslaw Swatek,<sup>1,2</sup> Benjamin Schruk,<sup>1,2</sup> Daixiang Mou,<sup>1,2</sup> Lunan Huang,<sup>1,2</sup> S. L. Bud'ko,<sup>1,2</sup> P. C. Canfield,<sup>1,2,\*</sup> and Adam Kaminski<sup>1,2,†</sup>

<sup>1</sup>*Division of Materials Science and Engineering, Ames Laboratory, Ames, Iowa 50011, USA*

<sup>2</sup>*Department of Physics and Astronomy, Iowa State University, Ames, Iowa 50011, USA*

<sup>3</sup>*Department of Materials Science and Engineering, Iowa State University, Ames, Iowa 50011, USA*

(Dated: August 13, 2018)

We use magnetization measurements, high-resolution angle-resolved photoemission spectroscopy (ARPES), and density functional theory (DFT) calculations to study the electronic properties of  $\text{Au}_2\text{Pb}$ , a topological superconductor candidate. The magnetization measurements reveal three discontinuities at 40, 51, and 99 K that agree well with reported structural phase transitions. To measure the band structure along desired crystal orientations, we utilized polishing, sputtering, and annealing to obtain clean flat sample surfaces. ARPES measurements of the  $\text{Au}_2\text{Pb}$  (111) surface at 110 K shows a shallow hole pocket at the center and flower-petal-like surface states at the corners of the Brillouin zone. These observations match the results of DFT calculations relatively well. The flower-petal-like surface states appear to originate from a Dirac like dispersion close to the zone corner. For the  $\text{Au}_2\text{Pb}$  (001) surface at 150 K, ARPES reveals at least one electron pocket between the  $\Gamma$  and  $M$  points, consistent with the DFT calculations. Our results provide evidence for the possible existence of Dirac state in this material.

The prediction<sup>1</sup> and observation<sup>2,3</sup> of the Dirac states on the surface of topological insulators have sparked a search for relativistic quasiparticles in condensed matter systems. Dirac fermions have been observed in three-dimensional (3D) Dirac semimetals such as  $\text{Cd}_3\text{As}_2$  and  $\text{Na}_3\text{Bi}$ <sup>4-6</sup>, where the Dirac points are protected by symmetry. By breaking the inversion<sup>7</sup> or time-reversal symmetry<sup>8</sup> in the Dirac fermion systems, Weyl fermion states can be realized. The observation of Fermi arc surface states, either in type-I<sup>7</sup> or type-II<sup>9-11</sup> Weyl semimetals, has been recognized as one of the distinct signatures of Weyl fermion states. In addition to the Dirac and Weyl fermions, another relativistic quasiparticle, namely the Majorana fermion is expected to occur at the intersection of superconductivity and topology.

The Majorana fermion state is fascinating because the quasiparticle is its own antiparticle and the bound state obeys non-Abelian statistics. This distinct feature makes it an excellent candidate for topological quantum computation<sup>12</sup>. One natural platform to realize Majorana fermions is topological superconductors. The topological nature guarantees that the gapless excitations at the surface satisfy the Dirac equation; whereas the superconducting nature guarantees that the particle-hole symmetry leads to indistinguishable particle-antiparticle<sup>13</sup>. There are several routes to realize topological superconductivity<sup>14</sup>. One route is to use the proximity effect<sup>15</sup>, such as placing ferromagnetic atomic chains on a superconductor<sup>16</sup>. Another route is to bring superconductivity to topological materials, such as doping topological insulator  $\text{Bi}_2\text{Se}_3$  with Cu<sup>17</sup>, or applying pressure to  $\text{Bi}_2\text{Se}_3$ <sup>18</sup>. However, this route suffers from difficulties in crystal synthesis, random distribution of impurities, or in ease of use for practical applications. A better route is to find stoichiometric single crystals that satisfy both topological property and superconductivity. Topological nodal line materials<sup>19-21</sup> have Dirac nodes forming a line or arc,

among which  $\text{PbTaSe}_2$  has been reported to show superconducting transition at  $T = 3.7 - 3.9 \text{ K}$ <sup>22,23</sup>. However, the Majorana fermion states in this material still remain elusive, possibly due to its extreme sensitivity to pressure<sup>23</sup>.

Recently,  $\text{Au}_2\text{Pb}$  has attracted attention because of the prediction of Dirac metal to topological metal transition at a structural phase change<sup>24</sup>, while the superconductivity of  $\text{Au}_2\text{Pb}$  has been reported more than fifty years ago<sup>25</sup>. With the topological transition accompanied by structural phase change,  $\text{Au}_2\text{Pb}$  offers a unique platform for studying the interplay of superconductivity, bulk Dirac states, and topological surface states in one single crystal<sup>24,26</sup>. However, until now, no angle-resolved photoemission spectroscopy (ARPES) measurements have provided direct evidence of topological states in this material.

Here, we present high-resolution ARPES data obtained from (001) and (111) surfaces that were prepared by polishing and several cycles of in-situ sputtering and annealing. We collect our ARPES data above 100 K so as to avoid any possible twinning effect associated with the structure transitions (see Fig. 1 below). The Fermi surface on the (111) facet consists of a shallow hole pocket at the  $\Gamma$  point and Fermi-arc-like surface states at the zone corners. On (001) surface, there is a Dirac like dispersion with a significant gap between the conduction and valence bands, consistent with the density functional theory (DFT) calculations.

Temperature and magnetization measurements were carried out using a Quantum Design Magnetic Property Measurement System (MPMS), superconducting quantum interference device (SQUID) magnetometer ( $T = 1.8 - 300 \text{ K}$ ,  $H_{max} = 55 \text{ kOe}$ ).

Large single crystalline samples of  $\text{Au}_2\text{Pb}$  were grown out of a high-temperature solution<sup>27,28</sup> rich in Pb. Stoichiometric quantities of elemental Au and Pb were mixed

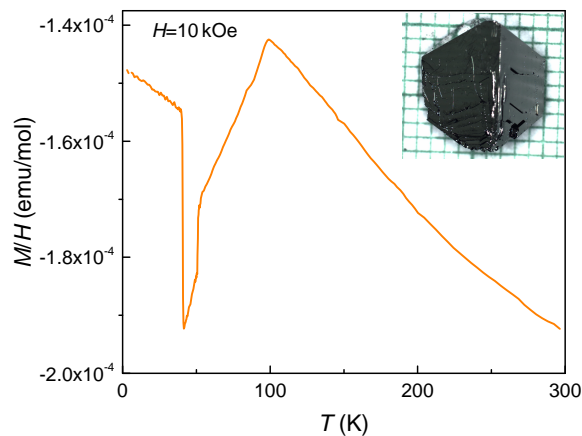


FIG. 1. (color online) Temperature dependent magnetization measurements of  $\text{Au}_2\text{Pb}$ . Inset shows the crystal with naturally grown (111) facets.

in molar ratios of  $\text{Au}_{40}\text{Pb}_{60}$ . The initial elements were placed into the bottom 2 ml alumina crucible of a Canfield Crucible Set<sup>29</sup>, and sealed in amorphous silica ampules under a partial argon atmosphere. The ampules were heated to 900 °C in 3 hours and dwelled there for 2 hours. The ampules were then rapidly cooled to 410 °C over 3 hours, followed by a slow cooling to 280 °C over 150 hours. At that point, the excess molten Pb-rich solution was decanted.

$\text{Au}_2\text{Pb}$  single crystals have naturally grown (111) facets (See inset to Fig. 1). Flat (001) surfaces of  $\text{Au}_2\text{Pb}$  were obtained by polishing Laue-oriented single crystals. Both surfaces for ARPES measurements were prepared by multiple cycles of annealing the single crystals below the melting point and sputtering in a  $10^{-5}$  Torr argon partial pressure. The ARPES measurements were performed using a helium discharge lamp based ARPES system consisting of a GammaData Helium ultraviolet lamp and a Scienta SES2002 electron analyzer. The angular and energy resolutions of this system were set at  $\sim 0.3^\circ$  and 15 meV, respectively.

Band structure with spin-orbit (SOC) included has been calculated in DFT<sup>30,31</sup> using PBE<sup>32</sup> exchange-correlation functional, a plane-wave basis set and projected augmented wave method<sup>33</sup> as implemented in VASP<sup>34,35</sup>. For bulk band structure of  $\text{Au}_2\text{Pb}$ , we used the primitive cell of 6 atoms with a Monkhorst-Pack<sup>36</sup> ( $13 \times 13 \times 13$ )  $k$ -point mesh including the  $\Gamma$  point and a kinetic energy cutoff of 230 eV. For surface band structure of  $\text{Au}_2\text{Pb}(111)$ , a unit cell of 18 atoms with a  $k$ -point mesh of ( $13 \times 13 \times 3$ ) is used. Experimental lattice parameters have been used with atoms fixed in their bulk positions. A tight-binding model based on maximally localized Wannier functions<sup>37–39</sup> was constructed to reproduce closely the bulk band structure including SOC in the range of  $E_F \pm 1$  eV with Au  $sd$  and Pb  $sp$  orbitals. Fermi surface and spectral functions of a semi-infinite  $\text{Au}_2\text{Pb}(111)$  surface were calculated with the sur-

face Green's function method<sup>40–43</sup> as implemented in WannierTools<sup>44</sup>. Different terminations of (111) surface have been calculated and we found that the Pb-dimer termination gives the best agreement to ARPES.

Figure 1 shows the temperature dependent magnetization measurement of a single crystal of  $\text{Au}_2\text{Pb}$ . Three discontinuities are seen at 40, 51, and 99 K, consistent with the previously reported structural phase transitions based on resistivity and specific heat data<sup>24</sup>.

Figure 2(a) shows the ARPES intensity integrated within 10 meV about the chemical potential measured on the sputtered and annealed  $\text{Au}_2\text{Pb}$  (111) surface. At the center of both the first and second Brillouin Zones (BZs), a shallow hole pocket can be clearly seen. Surrounding the center hole pocket are six flower-petal-like patterns originate from surface states, which is consistent with the crystal symmetry on this surface. Fig. 2(b) shows the calculation of  $\text{Au}_2\text{Pb}$  (111) surface, which matches relatively well the experimental results. Detailed band structure of  $\text{Au}_2\text{Pb}$  are plotted in Figs. 2(c)–(j), corresponding to the cuts along #1 to #4 in panel (a). Through a detailed comparison between the ARPES data and DFT calculations, we can identify those high intensity bands in ARPES data as surface states. Figure 2(c) shows the band dispersion along cut #1 in Fig. 2(a), which is consistent with the surface calculations in Fig. 2(b), especially the parts enclosed by the red and black dashed squares in either figure. The wider band dispersion of the surface states in experimental data than DFT calculations can be due to the absence of ionic relaxation effect in DFT calculations<sup>45,46</sup>. More details of the flower petal surface state are shown in Figs. 2(e) and (f) along cut #2. One can clearly see the surface states emerging from the bulk states and crossing the Fermi level in both the ARPES and surface calculation data, where a possible bulk Dirac dispersion can be identified. The missing parabolic band in ARPES data at  $k_2 = 0$  is most likely due to the matrix element effect. For cuts #3 and #4, the ARPES data and surface calculations show strong consistency except a 80 meV shift of the chemical potential, probably due to the Pb vacancy defects observed in this material<sup>47</sup>.

Figure 3 presents the features observed on the  $\text{Au}_2\text{Pb}$  (111) surface. As shown in Fig. 3(a), the flower-petal surface state seems to terminate and merge into the bulk states. The second derivative of (a) shows that the surface state may terminate before merging into the bulk states, leading to possible Fermi arc surface states<sup>48</sup>. Fermi arc surface state is one of the distinct signatures of Weyl semimetals, which has also been observed in 3D Dirac semimetal  $\text{Na}_3\text{Bi}$ <sup>49</sup>. Thus, the observation of Fermi arc-like surface states in  $\text{Au}_2\text{Pb}$  provides evidence for the possible existence of 3D Dirac states, as proposed in Ref. 24. At higher binding energies, the intensity of the Fermi surface part enclosed by red dashed circle in Fig. 3(b) shrinks down to a single point in Fig. 3(c) and expands again to a rough circle in Fig. 3(d). This is consistent with the Dirac-like feature in band dispersion shown in Fig. 3(i) and even better visualized in the

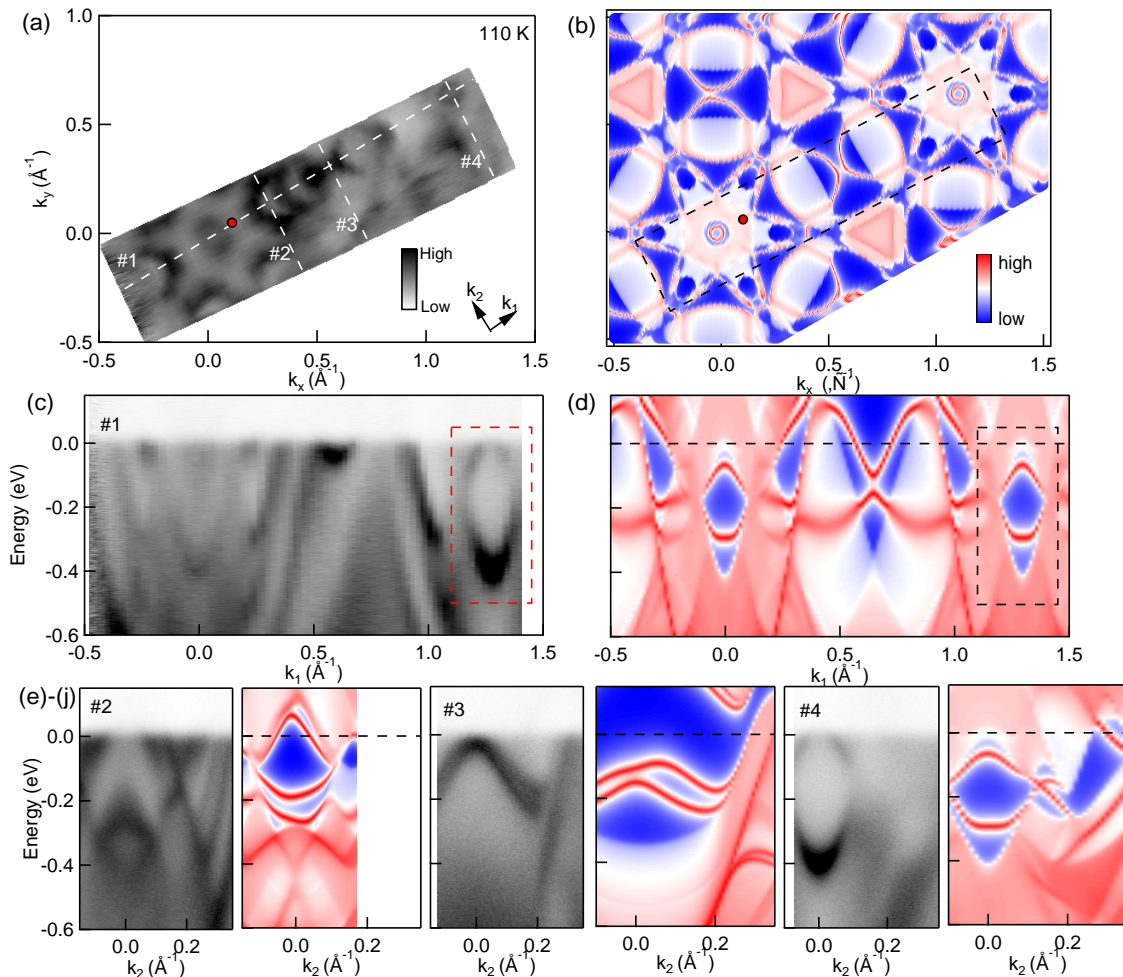


FIG. 2. (color online) Fermi surface and band dispersions of  $\text{Au}_2\text{Pb}$  (111) surface. (a) Fermi surface plot at 110 K - ARPES intensity integrated within 10 meV about the chemical potential. (b) Calculation of  $\text{Au}_2\text{Pb}$  (111) surface with Pb-dimer termination at 80 meV below chemical potential. Note: red dots in (a) and (b) are shown to provide reference location of the Dirac point from DFT calculations. Dashed box is region of data shown in (a). (c)–(j) ARPES intensity and surface band calculations along cuts #1 to #4 in (a). Red and black dashed boxes in (c) and (d) show consistency between ARPES and DFT calculations.

second-derivative image shown in Fig. 3(j).

Figure 4 shows the Fermi surface and band dispersion measured on the polished  $\text{Au}_2\text{Pb}$  (001) surface. At almost quarter way between  $\Gamma$  and  $M$  points, an electron pocket can be clearly observed. As we further approaching the  $M$  point, another larger pocket can be seen. These observations are consistent with the DFT calculations shown in Fig. 4(b), where the black dashed line encloses the area shown in panel (a). The band dispersion along the white dashed line in (a) is shown in Fig. 4(c), where a Dirac like dispersion can be better visualized in its second derivative image [Fig. 4(d)]. This also matches the result from DFT calculations as shown in Fig. 4(e), except that fewer bands can be observed in the ARPES measurements. This band dispersion also shows a significant gap between the conduction and valence bands, which can be demonstrated by the energy

distribution curve (EDC) [Fig. 4(d)] along the red dashed line in 4(c). A gap size of 200 meV can be estimated by the peak positions in the EDC. Since we only obtained adequate ARPES intensity at a  $k$  value off the calculated Dirac point [black solid circle in 4(b)], we cannot directly approve the existence of Dirac state in this material. On the other hand, the consistency between the Fermi surface/band dispersion and the band structure calculations point to the possible existence of 3D Dirac state on  $\text{Au}_2\text{Pb}$  (001) surface.

In conclusion, we used magnetization measurements, high-resolution ARPES system, and DFT calculations to investigate the electronic structure of  $\text{Au}_2\text{Pb}$  single crystals on (111) and (001) surfaces. Three discontinuities can be clearly seen in the magnetization measurements, consistent with the reported structural phase transitions. Interestingly, we observed Dirac-like disper-

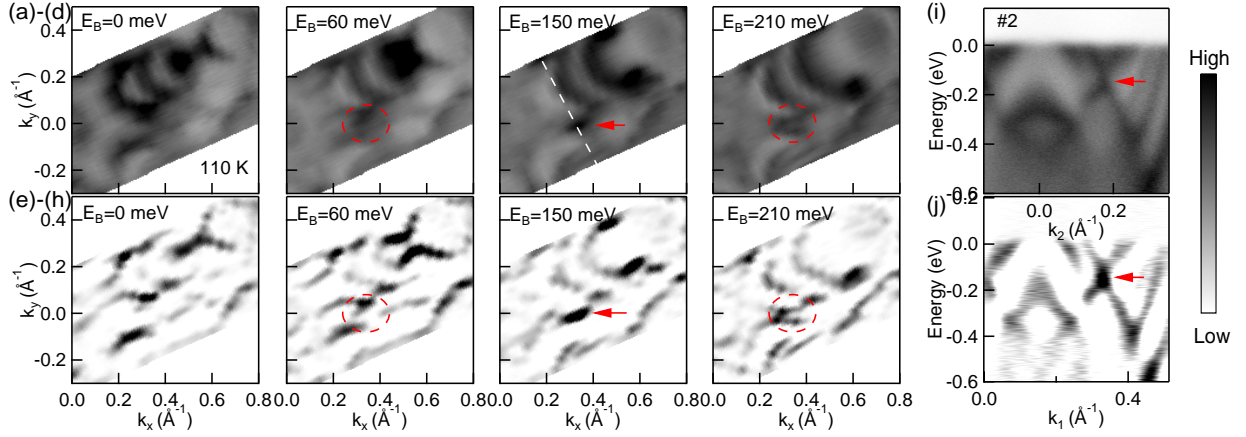


FIG. 3. (color online) Constant-energy contours and band dispersion of  $\text{Au}_2\text{Pb}$  (111) surface measured at 110 K. (a)–(d) ARPES intensity integrated within 10 meV at the binding energy of 0, 60, 150, and 210 meV, respectively. (e)–(h) Second-derivative images of (a)–(d), respectively. (i) band dispersion along white dashed line in (c). (j) Second-derivative image of (i). The red dashed circles in (b),(d), (f), and (h) enclose the part of the Dirac-like dispersion. The red arrows in (c), (g), (i), and (j) point to the Dirac-like point.

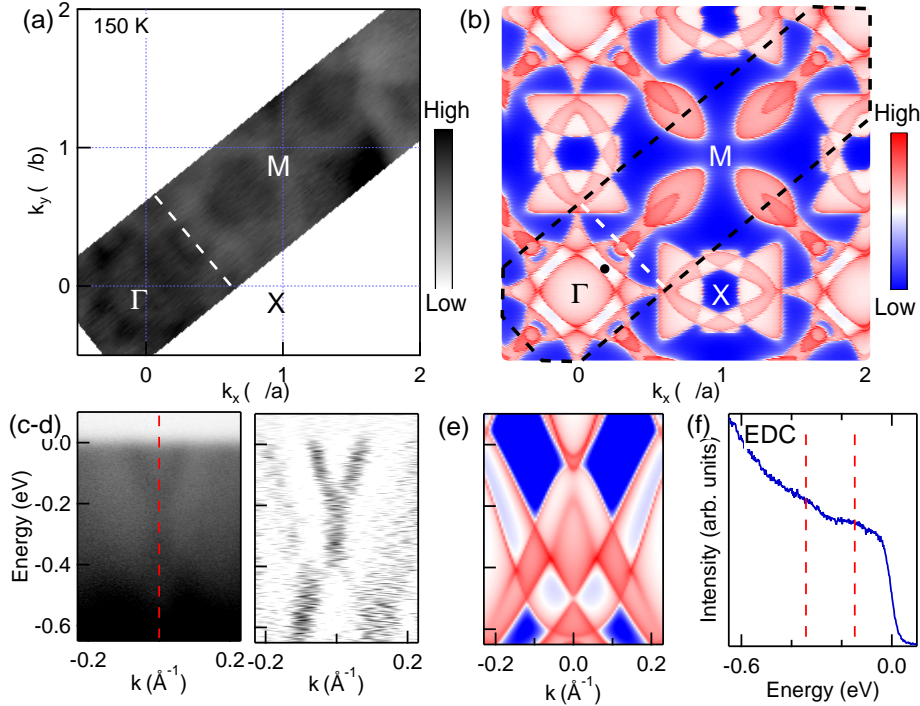


FIG. 4. (color online) Fermi surface and band dispersion of  $\text{Au}_2\text{Pb}$  (001) surface measured at 150 K. (a) Fermi surface plot - ARPES intensity integrated within 10 meV about the chemical potential. (b) Calculated bulk Fermi surface of  $\text{Au}_2\text{Pb}$  (001) surface. The black dashed line encloses the area of ARPES measurement in (a). (c) Band dispersion along the white dashed line in (a). (d) Second-derivative image of (c). (e) Calculated band dispersion along the white dashed line in (b). (f) Energy distribution curve (EDC) along the red dashed line in (c).

sion on polished  $\text{Au}_2\text{Pb}$  (111) surface with Fermi arc-like surface states. These results are consistent with the surface band-structure calculations. Furthermore, on  $\text{Au}_2\text{Pb}$  (001) surface, we observed a gapped Dirac-like dispersion. These observations point to the possible

topological nature of this material. However, due to the low superconducting transition temperature, we are not able to investigate the potential topological superconductivity in this material. Further study would require better prepared crystal surfaces, and ultralow temperature

systems. To conclude, our results and technique to obtain a clean surface on desired crystal orientations pave the way for further exploring the topological superconducting property in this material and make it an ideal candidate for studies of Majorana Fermions using scanning tunneling microscopy<sup>16</sup> etc.

Research was supported by the U.S. Department of Energy, Office of Basic Energy Sciences, Division of Materials Science and Engineering. Ames Laboratory is op-

erated for the U.S. Department of Energy by Iowa State University under Contract No. DE-AC02-07CH11358. Y. W. and L. L. W. were partially supported by Ames Laboratory's Laboratory-Directed Research and Development (LDRD) funding. G. D. was supported by the Gordon and Betty Moore Foundation EPiQS Initiative (Grant No. GBMF4411). B. S. and L. H. were supported by CEM, a NSF MRSEC, under Grant No. DMR-1420451.

Raw data for this manuscript is available at<sup>50</sup>.

\* canfield@ameslab.gov

† kaminski@ameslab.gov

- <sup>1</sup> H. Zhang, C.-X. Liu, X.-L. Qi, X. Dai, Z. Fang, and S.-C. Zhang, *Nat. Phys.* **5**, 438 (2009).
- <sup>2</sup> Y. Xia, D. Qian, D. Hsieh, L. Wray, A. Pal, H. Lin, A. Bansil, D. Grauer, Y. S. Hor, R. J. Cava, and M. Z. Hasan, *Nat. Phys.* **5**, 398 (2009).
- <sup>3</sup> Y. L. Chen, J. G. Analytis, J.-H. Chu, Z. K. Liu, S.-K. Mo, X. L. Qi, H. J. Zhang, D. H. Lu, X. Dai, Z. Fang, S. C. Zhang, I. R. Fisher, Z. Hussain, and Z.-X. Shen, *Science* **325**, 178 (2009).
- <sup>4</sup> Z. K. Liu, B. Zhou, Y. Zhang, Z. J. Wang, H. M. Weng, D. Prabhakaran, S.-K. Mo, Z. X. Shen, Z. Fang, X. Dai, Z. Hussain, and Y. L. Chen, *Science* **343**, 864 (2014).
- <sup>5</sup> M. Neupane, S. Xu, R. Sankar, N. Alidoust, G. Bian, C. Liu, I. Belopolski, T. Chang, H. Jeng, H. Lin, A. Bansil, F. Chou, and M. Z. Hasan, *Nat Commun* **5** (2014).
- <sup>6</sup> Z. K. Liu, J. Jiang, B. Zhou, Z. J. Wang, Y. Zhang, H. M. Weng, D. Prabhakaran, S.-K. Mo, H. Peng, P. Dudin, T. Kim, M. Hoesch, Z. Fang, X. Dai, Z. X. Shen, D. L. Feng, Z. Hussain, and Y. L. Chen, *Nat Mater* **13**, 677 (2014).
- <sup>7</sup> S.-Y. Xu, I. Belopolski, N. Alidoust, M. Neupane, G. Bian, C. Zhang, R. Sankar, G. Chang, Z. Yuan, C.-C. Lee, S.-M. Huang, H. Zheng, J. Ma, D. S. Sanchez, B. Wang, A. Bansil, F. Chou, P. P. Shibayev, H. Lin, S. Jia, and M. Z. Hasan, *Science* **349**, 613 (2015).
- <sup>8</sup> Z. Wang, M. G. Vergniory, S. Kushwaha, M. Hirschberger, E. V. Chulkov, A. Ernst, N. P. Ong, R. J. Cava, and B. A. Bernevig, *Phys. Rev. Lett.* **117**, 236401 (2016).
- <sup>9</sup> L. Huang, T. M. McCormick, M. Ochi, Z. Zhao, M. Suzuki, R. Arita, Y. Wu, D. Mou, H. Cao, J. Yan, N. Trivedi, and A. Kaminski, *Nat Mater* **15**, 1155 (2016).
- <sup>10</sup> A. Tamai, Q. S. Wu, I. Cucchi, F. Y. Bruno, S. Riccò, T. K. Kim, M. Hoesch, C. Barreateau, E. Giannini, C. Besnard, A. A. Soluyanov, and F. Baumberger, *Phys. Rev. X* **6**, 031021 (2016).
- <sup>11</sup> K. Deng, G. Wan, P. Deng, K. Zhang, S. Ding, E. Wang, M. Yan, H. Huang, H. Zhang, Z. Xu, J. Denlinger, A. Fedorov, H. Yang, W. Duan, H. Yao, Y. Wu, S. Fan, H. Zhang, X. Chen, and S. Zhou, *Nat Phys* **12**, 1105 (2016).
- <sup>12</sup> C. Nayak, S. H. Simon, A. Stern, M. Freedman, and S. Das Sarma, *Rev. Mod. Phys.* **80**, 1083 (2008).
- <sup>13</sup> M. Sato and Y. Ando, *Reports on Progress in Physics* **80**, 076501 (2017).
- <sup>14</sup> C. Beenakker and L. Kouwenhoven, *Nat Phys* **12**, 618 (2016).
- <sup>15</sup> L. Fu and C. L. Kane, *Phys. Rev. Lett.* **100**, 096407 (2008).

- <sup>16</sup> S. Nadj-Perge, I. K. Drozdov, J. Li, H. Chen, S. Jeon, J. Seo, A. H. MacDonald, B. A. Bernevig, and A. Yazdani, *Science* **346**, 602 (2014).
- <sup>17</sup> Y. S. Hor, A. J. Williams, J. G. Checkelsky, P. Roushan, J. Seo, Q. Xu, H. W. Zandbergen, A. Yazdani, N. P. Ong, and R. J. Cava, *Phys. Rev. Lett.* **104**, 057001 (2010).
- <sup>18</sup> K. Kirshenbaum, P. S. Syers, A. P. Hope, N. P. Butch, J. R. Jeffries, S. T. Weir, J. J. Hamlin, M. B. Maple, Y. K. Vohra, and J. Paglione, *Phys. Rev. Lett.* **111**, 087001 (2013).
- <sup>19</sup> G. Bian, T. Chang, R. Sankar, S. Xu, H. Zheng, T. Neupert, C. Chiu, S. Huang, G. Chang, I. Belopolski, D. S. Sanchez, M. Neupane, N. Alidoust, C. Liu, B. Wang, C. Lee, H. Jeng, C. Zhang, Z. Yuan, S. Jia, A. Bansil, F. Chou, H. Lin, and M. Z. Hasan, *Science* **346**, 1109 (2016).
- <sup>20</sup> Y. Wu, L. Wang, E. Mun, D. D. Johnson, D. Mou, L. Huang, Y. Lee, S. L. Bud'ko, P. C. Canfield, and A. Kaminski, *Nat Phys* **12**, 667 (2016).
- <sup>21</sup> L. M. Schoop, M. N. Ali, C. Straszler, A. Topp, A. Varykhalov, D. Marchenko, V. Duppel, S. S. P. Parkin, B. V. Lotsch, and C. R. Ast, *Nat Commun* **7**, 11696 (2016).
- <sup>22</sup> M. N. Ali, Q. D. Gibson, T. Klimczuk, and R. J. Cava, *Phys. Rev. B* **89**, 020505 (2014).
- <sup>23</sup> U. S. Kaluarachchi, Y. Deng, M. F. Besser, K. Sun, L. Zhou, M. C. Nguyen, Z. Yuan, C. Zhang, J. S. Schilling, M. J. Kramer, S. Jia, C.-Z. Wang, K.-M. Ho, P. C. Canfield, and S. L. Bud'ko, *Phys. Rev. B* **95**, 224508 (2017).
- <sup>24</sup> L. M. Schoop, L. S. Xie, R. Chen, Q. D. Gibson, S. H. Lapidus, I. Kimchi, M. Hirschberger, N. Haldolaarachchige, M. N. Ali, C. A. Belvin, T. Liang, J. B. Neaton, N. P. Ong, A. Vishwanath, and R. J. Cava, *Phys. Rev. B* **91**, 214517 (2015).
- <sup>25</sup> D. Hamilton, C. Raub, B. Matthias, E. Corenzwit, and G. Hull, *Journal of Physics and Chemistry of Solids* **26**, 665 (1965).
- <sup>26</sup> Y. Xing, H. Wang, C. Li, X. Zhang, J. Liu, Y. Zhang, J. Luo, Z. Wang, Y. Wang, L. Ling, M. Tian, S. Jia, J. Feng, X. Liu, J. Wei, and J. Wang, *Npj Quantum Materials* **1**, 16005 (2016).
- <sup>27</sup> P. C. Canfield and I. R. Fisher, *J. Crys. Growth* **225**, 155 (2001).
- <sup>28</sup> P. C. Canfield and Z. Fisk, *Philosophical Magazine Part B* **65**, 1117 (1992).
- <sup>29</sup> P. C. Canfield, T. Kong, U. S. Kaluarachchi, and N. H. Jo, *Philosophical Magazine* **96**, 84 (2016).
- <sup>30</sup> P. Hohenberg and W. Kohn, *Phys. Rev.* **136**, B864 (1964).
- <sup>31</sup> W. Kohn and L. J. Sham, *Phys. Rev.* **140**, A1133 (1965).
- <sup>32</sup> J. P. Perdew, K. Burke, and M. Ernzerhof, *Phys. Rev.*

- Lett. **77**, 3865 (1996).
- <sup>33</sup> P. E. Blöchl, Phys. Rev. B **50**, 17953 (1994).
- <sup>34</sup> G. Kresse and J. Furthmüller, Phys. Rev. B **54**, 11169 (1996).
- <sup>35</sup> G. Kresse and J. Furthmüller, Computational Materials Science **6**, 15 (1996).
- <sup>36</sup> H. J. Monkhorst and J. D. Pack, Phys. Rev. B **13**, 5188 (1976).
- <sup>37</sup> N. Marzari and D. Vanderbilt, Phys. Rev. B **56**, 12847 (1997).
- <sup>38</sup> I. Souza, N. Marzari, and D. Vanderbilt, Phys. Rev. B **65**, 035109 (2001).
- <sup>39</sup> N. Marzari, A. A. Mostofi, J. R. Yates, I. Souza, and D. Vanderbilt, Rev. Mod. Phys. **84**, 1419 (2012).
- <sup>40</sup> D. H. Lee and J. D. Joannopoulos, Phys. Rev. B **23**, 4988 (1981).
- <sup>41</sup> D. H. Lee and J. D. Joannopoulos, Phys. Rev. B **23**, 4997 (1981).
- <sup>42</sup> M. P. L. Sancho, J. M. L. Sancho, and J. Rubio, Journal of Physics F: Metal Physics **14**, 1205 (1984).
- <sup>43</sup> M. P. L. Sancho, J. M. L. Sancho, J. M. L. Sancho, and J. Rubio, Journal of Physics F: Metal Physics **15**, 851 (1985).
- <sup>44</sup> Q. Wu, S. Zhang, H.-F. Song, M. Troyer, and A. A. Soluyanov, arXiv preprint arXiv:1703.07789 (2017).
- <sup>45</sup> N. Fukui, T. Hirahara, T. Shirasawa, T. Takahashi, K. Kobayashi, and S. Hasegawa, Phys. Rev. B **85**, 115426 (2012).
- <sup>46</sup> M. V. Kuznetsov, L. V. Yashina, J. Sánchez-Barriga, I. I. Ogorodnikov, A. S. Vorokh, A. A. Volykhov, R. J. Koch, V. S. Neudachina, M. E. Tamm, A. P. Sirotina, A. Y. Varykhalov, G. Springholz, G. Bauer, J. D. Riley, and O. Rader, Phys. Rev. B **91**, 085402 (2015).
- <sup>47</sup> K. W. Chen, D. Graf, T. Besara, A. Gallagher, N. Kikugawa, L. Balicas, T. Siegrist, A. Shekhter, and R. E. Baumbach, Phys. Rev. B **93**, 045118 (2016).
- <sup>48</sup> I. Belopolski, S.-Y. Xu, D. S. Sanchez, G. Chang, C. Guo, M. Neupane, H. Zheng, C.-C. Lee, S.-M. Huang, G. Bian, N. Alidoust, T.-R. Chang, B. Wang, X. Zhang, A. Bansil, H.-T. Jeng, H. Lin, S. Jia, and M. Z. Hasan, Phys. Rev. Lett. **116**, 066802 (2016).
- <sup>49</sup> S.-Y. Xu, C. Liu, S. K. Kushwaha, R. Sankar, J. W. Krizan, I. Belopolski, M. Neupane, G. Bian, N. Alidoust, T.-R. Chang, H.-T. Jeng, C.-Y. Huang, W.-F. Tsai, H. Lin, P. P. Shibayev, F.-C. Chou, R. J. Cava, and M. Z. Hasan, Science **347**, 294 (2015).
- <sup>50</sup> [http://lib.dr.iastate.edu/ameslab\\_datasets/](http://lib.dr.iastate.edu/ameslab_datasets/).